VOL. 24, NO. 2, 2025, 141-148
elektrika.utm.my
ISSN 0128-4428

ELEKTRIKA
Journal of Electrical Engineering

Optimizing Q-Factor in 2D Photonic Crystal Nanocavity: Impact of Cavity Design and Cladding Materials

Muhammad Danial Haziq Azizan[1*], **Nurul Ashikin Daud**[1], **Asrul Izam Azmi**[1] and **Mohd Rashidi Salim**[1]

[1]Faculty of Electrical Engineering, Universiti Teknologi Malaysia, 81310 UTM Skudai, Johor, Malaysia.

[*]Corresponding author: md.haziq@graduate.utm.my

Abstract: Silicon-on insulator (SOI) photonic crystal (PhC) slabs are anticipated to play a critical role in advancing photonic devices for telecommunication and optical circuits. However, achieving high quality(Q)-factor and low mode volume remains a significant challenge in designing these structures. In this study, we propose a two-dimensional (2D) PhC structure by modulating the waveguide width and three different nanocavities formations created by shifting the selected air holes at the center of the structure. By using 3D finite-difference time-domain (FDTD) simulations, transmittance spectrum properties we analyzed. We have achieved the highest values of 2.07 $\times 10^6$ at 1.5447 μm for nanocavity shifted distance of 3 nm ,6 nm and 6 nm without cladding layer added. Furthermore, the challenge lies in minimizing the vertical scattering loss when different cladding materials are introduced. Through this simulation, we found that cladding layers impact the transmittance spectrum. The highest Q-factor is 1.41 $\times 10^6$ with mode volume of 0.826 if clad materials with silica (SiO_2). These findings demonstrate significant potential for integrating high-Q PhC structure into advanced optical devices, enhancing performance in telecommunication and photonic circuits.

Keywords: Photonic crystal (PhC), photonic bandgap (PBG), cladding, quality (Q) factor, mode volume

Article History: received 25 November 2024; accepted 23 December 2024; published 31 August 2025

1. INTRODUCTION

Recent advancement in photonic crystal (PhC) has led to a widespread interest across various optical devices [1]. While foundational work on the understanding of light can be traced back to pioneers like Alhazen and Newton, Lord Rayleigh's contributions in the early 20th century significantly advanced wave theory and scattering phenomena [2]. PhC has grown significantly from 1980s and 1990s, leading to the evolution of modern photonic applications by Eli Yablonovitch [3] and Sajeev John [4]. They have reported that PhC are capable of manipulating light based on their periodic dielectric structure by forbidden behavior in photonic bandgap (PBG) [5]. Among the three dimensions of PhC structure, 2D PhC are particularly advantageous due to their simpler, small size, easier for fabrication, and flexible design compared to three-dimensional (3D). Therefore, 2D PhC structures are widely used in optical communications and sensing. Their ability to confine and manipulate the light efficiently in a planar structure makes them high-performance in photonic devices.

In order to make the 2D PhC structure more functional, a cavity is introduced by creating the resonant mode that's allow for trapping and confinement of light at a certain wavelength. By introducing these cavities in 2D PhC structure, performance and efficiency of optical devices can be significantly enhanced. Thus, the Q-factor is one of the important parameters to measure this enhancement besides the mode volume. The invention for the combination of low-loss waveguide and high-Q microcavities was one of the technological achievements that made it possible to build all-optical switches [6], [7], [8] and sensor [9], [10], [11], [12]. However, designing the cavity in 2D PhC structures presents several technical challenges. These challenges must be addressed to maximize the Q-factor and minimize the mode volume. The design and fabrication processes also must be highly precise to minimize defects and imperfections that can lead to energy loss. Furthermore, high-Q nanocavities in PhC offer small size and high Q-factor values [13]. Addressing these challenges requires innovative approaches in material selection and structural design.

Recent breakthroughs have shown that adding cladding is an important part that will protect the 2D PhC structure due to its compact and small size. In addition, adding cladding also can reduce the scattering losses, which are common scenario in small-scale photonic devices. The common cladding materials used by previous researchers are silica (SiO_2) [13]-[15], silicon nitride (Si_3N_4), polymer-based and oxides. Each material has its own functionalities based on the application photonic devices. Hence, the choice of cladding materials must be carefully tailored to meet the specific performance requirements of the 2D PhC structure, ensuring optimal device functionality.

In this paper, we demonstrate the process to achieve

high Q-factor for 2D PhC structure by designing different cavity formations. The process begins by measuring the important characteristics such as bandgap and transmittance spectrum. By analyzing the resonance wavelength, cavities of this structure are introduced by shifting outwards the air holes direction from the waveguide at three different distances. Next, the Q-factor and mode volume are calculated based on the resonance wavelength that appears within the mode gap from transmittance spectrum simulation result. Lastly, this 2D PhC structure incorporates with three different cladding materials to observe their effects on the Q-factor and mode volume.

2. DESIGN

The design of 2D PhC involves precise selection material and geometrical structure to achieve an optimum performance. Therefore, Fig. 1 shows the proposed design with parameters of lattice constant, *a*, air holes radius, *r*, slab thickness, *t,* and waveguide width, *W*. For PhC slab material, Silicon (Si) was selected in this study due to its high refractive index contrast. In addition, this material also compatibility with complementary metal-oxide semiconductor (CMOS) process [13]-[19] for further fabrication process. This high refractive index contrast between Si and the air-clad results in a well-defined PBG which allows for a wide range of frequencies where light propagation is effectively suppressed. In addition, a hexagonal lattice is designed for the structure where can provide a significantly larger PBG for both transverse electric (TE) and transverse magnetic (TM) polarization [23]. The array of air holes is formed with a lattice constant, *a* of 420 nm and size of air holes radius, *r* is 128 nm. Then, the size of slab thickness, *t* is half the size of lattice constant which is 210 nm.

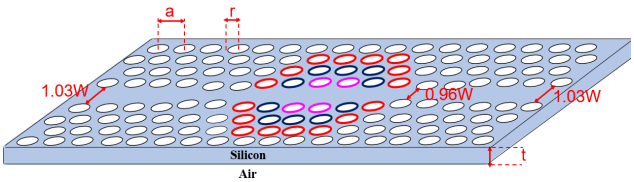

Figure 1. Schematic illustration of 2D PhC structure

In order to make sure light can propagate along the PhC structure, one array of air holes is removed in horizontal position to form a waveguide called as line defect. The size of this waveguide width is approximately to $\sqrt{3}a$. Therefore, by analyzing the band structure, the waveguide width modulated is applied at the input and output port that required about 3%, increase which is 1.03W of the actual size waveguide width. Then, to make light propagation thinner and narrower, the waveguide width at center of the waveguide will be reduced by about 4% (0.96W). By reducing it, the frequency shifts along waveguide and creating a mode gap appear at the cavity area.

The cavity is designed at the center of the waveguide by identifying the positions of the air holes surrounding the desired cavity location as shown in Fig. 2. These air holes are symmetrically shifted outwards from their initial location to form a resonant cavity. Fig. 3 shows three different distances of air holes shift. We shift air holes at the center of the PhC structure by 3 nm distance in outwards direction for the first, second and third air holes. This configuration is called as (3,3,3) nm air holes shift as illustrated in Fig. 3(a). Then, to analyze other cavity formation, the shifting air holes distance for second and third air holes are increased to 6 nm which is known as (3,6,6) nm air holes shift as illustrated in Fig. 3(b).

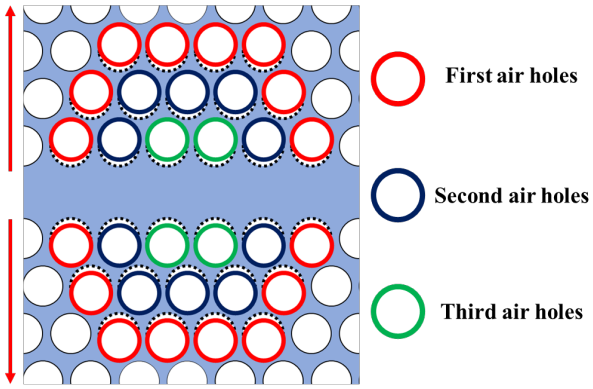

Figure 2. Location for first, second and third air holes for shifting outwards

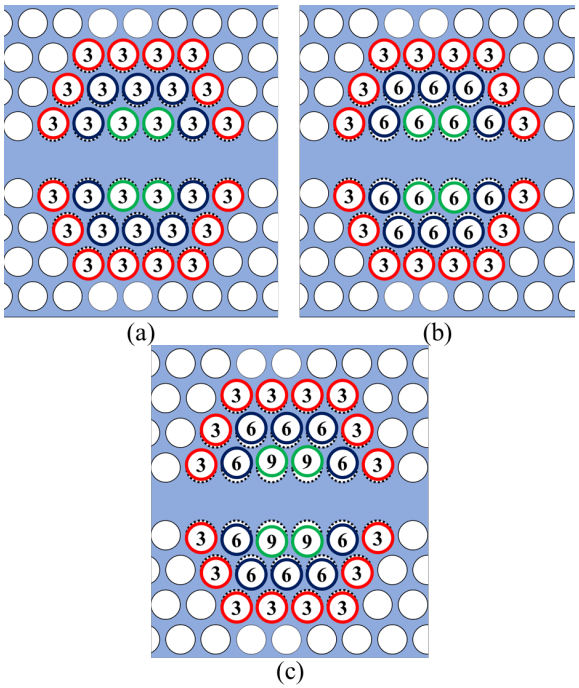

Figure 3. Type of shifting air holes to create the cavity in PhC structure (a) (3,3,3) nm, (b) (3,6,6) nm, and (c) (3,6,9) nm

Lastly, we increase the third air holes to 9 nm while maintaining the first and second air holes distance to 3 nm and 6 nm, respectively. We observed the effects on the resonance properties and the Q-factor of the cavity for the three different distance configurations of cavities.

3. RESULT AND DISCUSSION

The simulation results were obtained in MIT Photonic

Bands (MPB) open-source for bandgap and Lumerical software for transmittance spectrum properties. 3D finite-difference time-domain (FDTD) was used to employ the characteristics of the proposed design. We measured the bandgap, performance of Q-factor and mode volume based on 3 different shifting cavities of the structure. Then, we clad the structure with 3 different cladding materials to analyze the effect on the value of Q-factor.

3.1. Photonic Bandgap (PBG)

PBG is a range of frequencies in which light cannot propagate through a PhC structure due to the crystal's periodic structure by creating a forbidden zone [18], [20]. PBG is a useful characteristic in 2D planar structures as it is extremely sensitive to variations in critical structural parameters [24] such as the air holes radius, slab thickness, lattice constants, and refractive index of PhC slabs, waveguide width, and cladding.

Fig. 4 shows the bandgap that exists in the proposed PhC structure that allowed light at some frequency to be transmitted through the modulated waveguide of 1.03W. The bandgap for TE mode is polarised between normalized frequencies from 0.216 to 0.287 ($\omega a/2\pi c$). Hence, this shows that the proposed design structure allows light to propagate from 1.5 um to 1.7 um in the waveguide. By modulating the waveguide width at the input and output port to 1.03W, the mode gap can be shifted towards the lower normalized frequency.

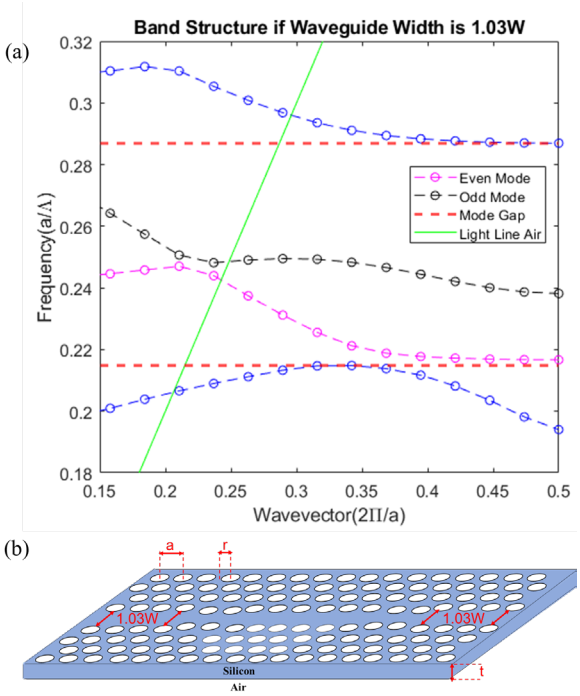

Figure 4. Bandgap structure for width modulated waveguide of 1.03W (a) PBG graph and (b) Location of 1.03W in 2D PhC structure

On the other hand, Fig. 5 shows the bandgap range appearing from 0.213 to 0.296 ($\omega a/2\pi c$) for the 0.96W waveguide. The odd and even modes are located at a higher frequency compared to the 1.03W waveguide. This is due to the changes of waveguide width that are from wider to narrower that have influenced the light modes frequency range. Note that, in this simulation, TE mode is used due to a larger bandgap compared to TM mode [25], [26]. Based on the electromagnetic spectrum, the range of wavelengths that are able to be transmitted in the waveguide is suitable to be operated for S-band, C-band, and L-band devices.

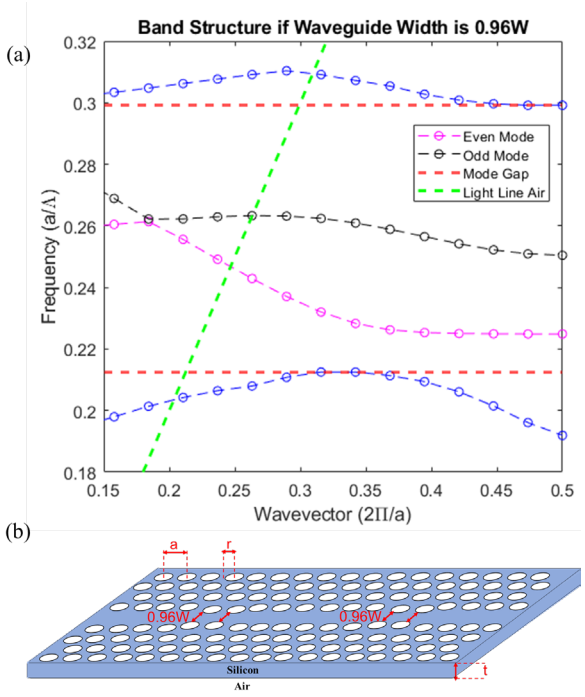

Figure 5. Bandgap structure for width modulated waveguide of 0.96W (a) PBG graph and (b) Location of 0.96W in 2D PhC structure

3.2. Transmittance Spectrum

Next, the transmittance spectrum of the proposed 2D PhC structure is analyzed. The performance of each cavity can be measured by calculating the value of Q-factor. From the transmittance spectrum, we analysed the resonance peak that appears within the mode gap. Q-factor is used to measure the efficiency of proposed cavity design in the PhC structure to confine light by quantifying the energy loss for a certain duration [27][28]. Q-factor is also used to measure the spectral width of a cavity's resonant peak. This relationship is crucial as it connects the temporal and spectral properties of the cavity.

$$Q = \frac{\lambda_0}{\Delta\lambda_{FWHM}} \; or \; \frac{f_0}{\Delta f_{FWHM}} \tag{1}$$

Equation (1) describes the formula used to measure the Q-factor, where λ_0 and f_0 are the resonance wavelength and resonance frequency of the peak, respectively. Besides that, $\Delta\lambda_{FWHM}$ and Δf_{FWHM} are interrelated to full width at half maximum (FWHM). The FWHM represents the width of the resonance peak at half of its maximum intensity, which is directly linked to energy loss within the cavity. By minimizing the FWHM, the Q-factor can be increased, indicating a more efficient PhC cavity.

The performance of the PhC cavity also can be measured by calculating the mode volume where there is a measurement of spatial confinement of the electromagnetic field within the cavity. Equation (2) describes the formula used to measure the mode volume where $E(x, y, z)$ is the electric field of optical cavity and ε is the permittivity of PhC material. A smaller mode volume signifies tighter confinement, which is beneficial for enhancing light-matter interactions.

$$V = \frac{\int\int\int \varepsilon|E(x,y,z)|^2 dxdydz}{max[\varepsilon|E(x,y,z)|^2]} \quad (2)$$

Based on equation (3), reducing the mode volume can lead to an increase in the interactivity strength between light and the material within the cavity. This enhancement is crucial for applications such as sensors and lasers, where strong light-matter interaction is desired. High Q-factor and small mode volume together contribute to the overall efficiency and performance of the PhC cavity.

$$High\ photon\ density = \frac{Q}{V} \quad (3)$$

Fig. 6 shows the simulated transmittance spectrum graph for different cavity configuration distances. By referring to Fig. 6(a), the resonance wavelength appears once the air holes shift outwards to (3,3,3) nm at the mode gap area that is from 1.53 µm to 1.56 µm. It shows that the resonance for (3,3,3) nm cavity configuration exhibits a wider width of FWHM, which is indicative of lower confinement efficiency and a broader width resonance. Hence, the value of Q-factor is 5.90×10^3 with a mode volume of 0.6471. Then, the position of the cavity is changed to the (3,6,6) nm cavity configuration as described in Fig. 3(b). By employing this cavity configuration, we observed a significant improvement in the Q-factor, which increased to 2.07×10^6 as shown in Fig. 6(b). Furthermore, the mode volume is slightly reduced to 0.6425. This reduction in mode volume implies a more effective confinement of the optical mode within the cavity as described in Equation 3.

Then, the cavity configuration is changed to (3,6,9) nm. Result in Fig. 6(c) shows the resonance wavelength appears at 1.546 µm with a value of Q-factor of 7.67×10^5 and a mode volume of 0.6420. Compared to the previous configurations in Fig.6 (a) and (b), this new arrangement shows that the resonance wavelength has slightly shifted to redshift wavelength. This configuration shows a promising result with improved light confinement and optimized optical properties. These results demonstrate that by precisely adjusting the positions of the air holes, we can achieve significant improvements in the Q-factor and enhance the overall performance of the photonic crystal cavity. This analysis emphasizes the importance of optimizing the cavity design to achieve higher Q-factors, which is crucial for applications requiring efficient light confinement and minimal energy loss.

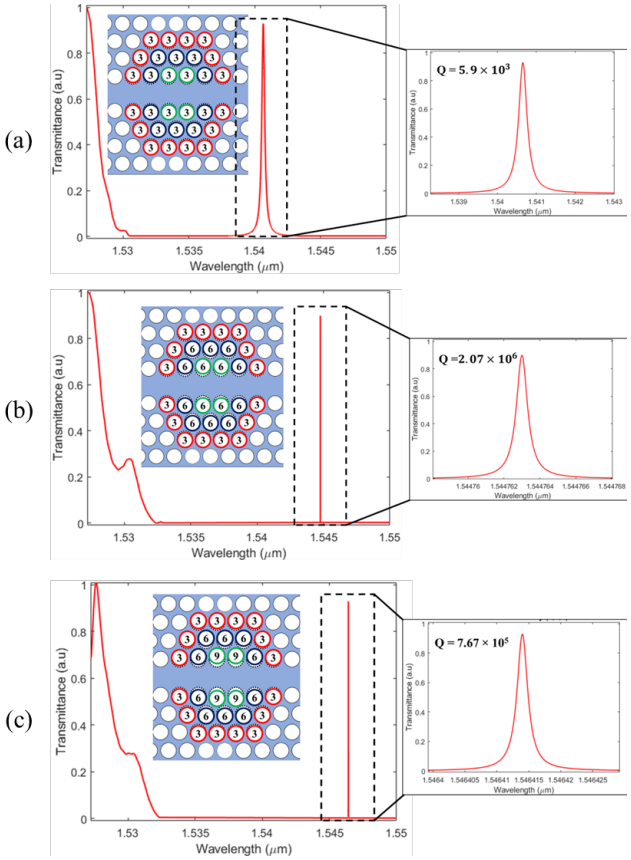

Figure 6. Transmittance spectrum graph with resonance wavelength for three different cavity configurations. (a) Transmittance spectrum for (3,3,3) nm cavity configuration obtained 5.90×10^3 value of Q-factor, (b) Transmittance spectrum for (3,6,6) nm cavity configuration obtained 2.70×10^6 value of Q-factor, and (c) Transmittance spectrum for (3,6,9) nm cavity configuration obtained 7.67×10^5 value of Q-factor

3.3. Cladding Materials

The 2D PhC slab has been explored by introducing the cladding materials in order to fabricate and protect the structure for photonic devices. There are few studies that thoroughly investigate the effects of different cladding on the Q-factor and mode volume.

Fig. 7 shows the illustration of a cladded 2D PhC slab with slab thickness, t_s and cladding thickness, t_c. Although generally, there is no specific cladding thickness to meet the application requirement, we set the t_c value to be 400 nm, which is 2 times thicker compared to the slab thickness to prevent vertical scattering leakage. We observed the three different clad materials that are SiO_2, Si_3N_4 and Al_2O_3 with their refractive indices of 1.44, 1.76, and 2.00, respectively. All these clad materials are compatible with the CMOS fabrication process.

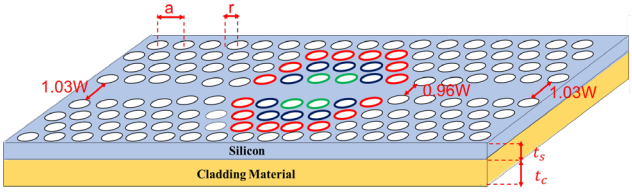

Figure 7. Schematic illustration of 2D PhC structure by

adding cladding materials

Fig. 8 shows the PBG for each clad material. The light line for each material represents the dispersion relation of light in the PhC waveguide, indicating their ability to propagate light effectively. Fig. 8 shows that all the clad material that is used in the proposed design structure appear at the mode gap range. This demonstrates that each cladding material can facilitate light propagation within the mode gap for 1.03W and 0.96W of waveguide width in the PhC structure. Therefore, this shows that the proposed design structure offers a versatility of cladding materials depending on applications and suitability.

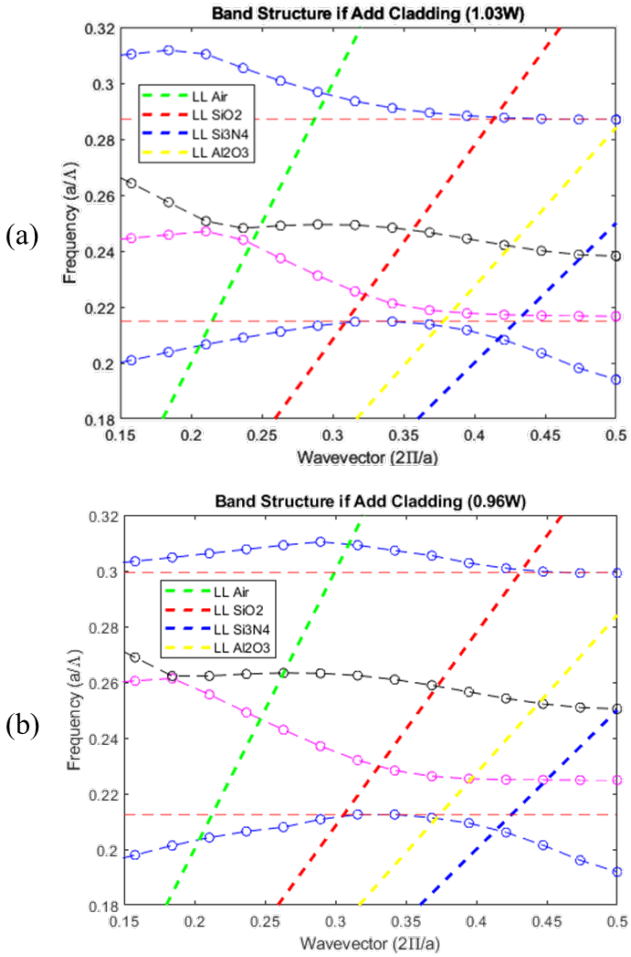

Figure 8. Bandgap graph for cladding materials if modulated waveguide width to (a) 1.03W and (b) 0.96W

Next, the effect for each cladding material is analyzed by measuring the Q-factor and mode volume. This analysis is conducted by comparing the differences between PhC cavity design configuration for different cladded materials with non-cladded structure.

When silica (SiO_2) cladding is added to the 2D PhC slab design for the cavity formation of (3,3,3) nm, the Q-factor decreases from 5.9×10^3 to 4.7×10^3 as shown in Fig. 9(a). The value of Q-factor keeps decreasing when the clad material is changed to aluminum oxide (Al_2O_3) and silicon nitride (Si_3N_4). The same patterns of results were obtained for different configurations of cavity structure, as shown in Fig. 9 (b) and (c). Therefore, these results prove that by cladded PhC slab, reduce the value of cavity's Q-factor [29]. However, in order to integrate the structure with other photonic devices in one circuit, SiO_2 has proven to be the best material compared to Al_2O_3 and Si_3N_4.

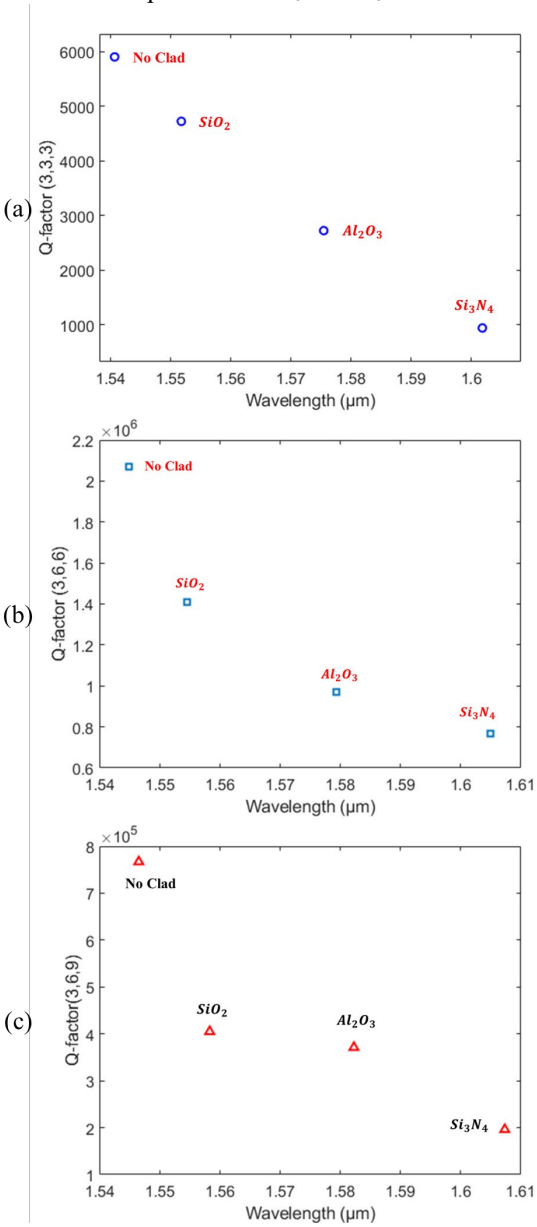

Figure 9. Q-factor vs wavelength for different cladding materials based on cavity (a) shifting air holes to 3nm, 3nm, 3nm, (b) shifting air holes 3nm, 6nm, 6nm, and (c) shifting air holes to 3nm, 6nm, 9nm

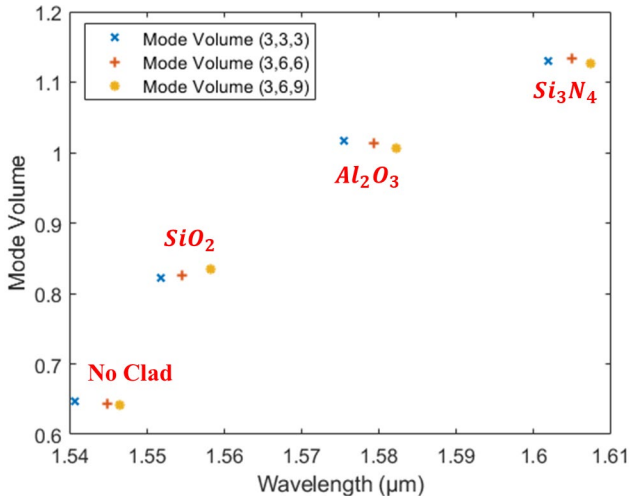

Figure 10. Mode volume vs wavelength for each cladding material based on 3 cavity formation

Fig. 10 focuses on the mode volume, denoted in units of $(\lambda/n)^3$, which describes the spatial extent of the optical mode within the cavity. Based on Eq. 3, there is an inverse relationship between the mode volume and Q-factor in this case. A higher mode volume in PhC required a larger region that led to a decrease in photon confinement within the cavity. As a result, the Q-factor which measures the performance of the cavity intends to decrease as shown in Fig. 10.

Hence, Table 1 provides a comparative analysis of different cladding types on the performance metrics of Q-factor and mode volume in various PhC cavity configurations. The table highlights significant variations in Q-factor values across different cavity designs, emphasizing the influence of cladding materials and thicknesses on light confinement and efficiency within the photonic structures. The previous study [14] has shown that by cladding silica to a silicon slab, a higher Q-factor, 1.7×10^6 can be obtained. The cavity of H0 is used by shifting the 5 air holes away to form resonant. The normal range for cladding thickness used is from 200nm to 400nm. Each cladding thickness will give a different result, especially on the resonance wavelength, which will redshift. Then, another research also has reported [15] that if using cladding thickness in ratio of 0.9, the Q-factor will gain to a higher value. Cladding is a very important aspect that needs to be considered once fabrication which is to protect the PhC structure. Hence, the choice of cladding thickness and materials is a very significant process to consider. Lastly, this work has obtained that adding the cladding cannot enhance the Q-factor even though it uses different materials that are compatible with CMOS process. The highest Q-factor has achieved is using cavity formation of (3,6,6)nm without any cladding, Q-factor of 2.07×10^6. Based on the result, we have successfully simulated this 2D PhC structure with different shifting air holes, including the materials for cladding.

Table 1. Comparison between the type of cladding towards the performance of Q-factor and mode volume

Ref.	Type of Cavities	Structure Materials	Cladding Material	Q-Factor	Mode Volume $(\lambda/n)^3$
[14]	Modify of H0 cavity by shifting away 5 crystals away	Si	SiO_2	1.7×10^6	1.34
[15]	L3 cavity	Si	SiO_2	2.5×10^3	-
[16]	Nanobeam cavity	AlN	SiO_2	1.1×10^6	-
[30]	L4/3 cavity	Si	SiO_2	20.9×10^6	0.32
[22]	Line defect with different lattice constant	Si	SiO_2	5.9×10^5	-
[31]	Combination of point defect and 2 waveguides	Si	No clad	5.3×10^4	-
This Work	Shifting air holes outwards to (3,6,6) nm	Si	No Clad SiO_2 Al_2O_3 Si_3N_4	2.07×10^6 1.41×10^6 9.7×10^5 7.66×10^5	0.6425 0.8260 1.0135 1.1343

4. CONCLUSION

In conclusion, research on 2D PhC has shown significant progress and potential in the field of photonics. Through meticulous design processes, light can propagate through the modulated waveguide width due to the presence of odd and even modes in the PBG. Among the three different cavity configurations, the (3,6,6) nm cavity configuration exhibits the highest Q-factor and lowest mode volume. The study has proven that SiO_2 is the best material for cladding the structure as it will not degrade the value of Q-factor 1.41×10^6,which indicates strong light confinement in the proposed structure. Therefore, this has proven that the proposed design structure has potential to be fabricated and applied as optical switching devices.

ACKNOWLEDGMENT

This work was funded by the Ministry of Higher Education under Fundamental Research Grant Scheme (FRGS/1/2022/TK07/UTM/02/61) and Universiti Teknologi Malaysia for the funding under UTM Fundamental Research (UTMFR) (Q.J130000.3851.22H05).

REFERENCES

[1] M. A. Butt, S. N. Khonina, and N. L. Kazanskiy, "Recent advances in photonic crystal optical devices: A review," *Opt Laser Technol*, vol. 142, p. 107265, Oct. 2021, doi: 10.1016/j.optlastec.2021.107265.

[2] Lord Rayleigh, "XXVI. *On the remarkable phenomenon of crystalline reflexion described by* Prof. Stokes," *The London, Edinburgh, and Dublin Philosophical Magazine and Journal of Science*, vol. 26, no. 160, pp. 256–265, Sep. 1888, doi: 10.1080/14786448808628259.

[3] E. Yablonovitch, "Inhibited Spontaneous Emission in Solid-State Physics and Electronics," *Phys Rev Lett*, vol. 58, no. 20, pp. 2059–2062, May 1987, doi: 10.1103/PhysRevLett.58.2059.

[4] M. D. Al-Amri, M. El-Gomati, and M. S. Zubairy, Eds., *Optics in Our Time*. Cham: Springer International Publishing, 2016. doi: 10.1007/978-3-319-31903-2.

[5] S. John, "Strong localization of photons in certain disordered dielectric superlattices," *Phys Rev Lett*, vol. 58, no. 23, pp. 2486–2489, Jun. 1987, doi: 10.1103/PhysRevLett.58.2486.

[6] M. Takiguchi *et al.*, "All-Optical Switching using a III-V Nanowire Integrated Si Photonic Crystal Nanocavity," in *2019 IEEE Photonics Conference (IPC)*, 2019, pp. 1–2. doi: 10.1109/IPCon.2019.8908286.

[7] X. Gao, Y. Wang, W. Gu, W. Dong, and X. Zhang, "High-Performance Thermo-Optic Switch Based on Graphene Microheater and Fano Slab Photonic Crystal Cavity," in *2023 Asia Communications and Photonics Conference/2023 International Photonics and Optoelectronics Meetings (ACP/POEM)*, 2023, pp. 1–4. doi: 10.1109/ACP/POEM59049.2023.10369345.

[8] Q. Saudan *et al.*, "Low-Power Thermo-Optic Switching Using Photonic Crystal Fano Structure with p-i-n Junction," in *2019 21st International Conference on Transparent Optical Networks (ICTON)*, 2019, pp. 1–4. doi: 10.1109/ICTON.2019.8840273.

[9] M. F. Bado and J. R. Casas, "A Review of Recent Distributed Optical Fiber Sensors Applications for Civil Engineering Structural Health Monitoring," *Sensors*, vol. 21, no. 5, p. 1818, Mar. 2021, doi: 10.3390/s21051818.

[10] J. Ye, "Optic fiber magnetic field sensor based on the miniature pull-taper twin-core photonic crystal fiber," in *14th International Photonics and Optoelectronics Meetings (POEM 2022)*, P. Shen, X. Zhang, and J. Dong, Eds., SPIE, Apr. 2023, p. 49. doi: 10.1117/12.2672693.

[11] Y. E. Monfared, R. Khosravi, M. Hajati, B. Kacerovska, P. Ma, and C. Liang, "Sensitive Temperature Sensors based on High Birefringence Liquid-Filled Photonic Crystal Fibers," in *2019 Photonics North (PN)*, IEEE, May 2019, pp. 1–1. doi: 10.1109/PN.2019.8819520.

[12] M. A. Butt, N. L. Kazanskiy, and S. N. Khonina, "Modal Characteristics of Refractive Index Engineered Hybrid Plasmonic Waveguide," *IEEE Sens J*, vol. 20, no. 17, pp. 9779–9786, Sep. 2020, doi: 10.1109/JSEN.2020.2991215.

[13] T. Tanabe, T. Tetsumoto, Y. Ooka, and Nurul Ashikin Binti Daud, "Recent progress on high-Q photonic crystal nanocavities: Photolithographic fabrication and reconfigurable system," in *2016 Progress in Electromagnetic Research Symposium (PIERS)*, IEEE, Aug. 2016, pp. 782–782. doi: 10.1109/PIERS.2016.7734464.

[14] U. P. Dharanipathy, M. Minkov, M. Tonin, V. Savona, and R. Houdré, "High-Q silicon photonic crystal cavity for enhanced optical nonlinearities," *Appl Phys Lett*, vol. 105, no. 10, Sep. 2014, doi: 10.1063/1.4894441.

[15] L. Kassa-Baghdouche, T. Boumaza, E. Cassan, and M. Bouchemat, "Enhancement of Q-factor in SiN-based planar photonic crystal L3 nanocavity for integrated photonics in the visible-wavelength range," *Optik (Stuttg)*, vol. 126, no. 22, pp. 3467–3471, Nov. 2015, doi: 10.1016/j.ijleo.2015.07.150.

[16] E. G. Melo, M. N. P. Carreño, and M. I. Alayo, "High-Q and Small Mode-Volume Oxide-Cladding Aluminum Nitride Photonic Crystal Nanocavity," in *Frontiers in Optics 2016*, Washington, D.C.: OSA, 2016, p. JTh2A.156. doi: 10.1364/FIO.2016.JTh2A.156.

[17] A. A. González-Fernández, W. W. Hernández-Montero, J. Hernández-Betanzos, C. Domínguez, and M. Aceves-Mijares, "Refractive index sensing using a Si-based light source embedded in a fully integrated monolithic transceiver," *AIP Adv*, vol. 9, no. 12, Dec. 2019, doi: 10.1063/1.5130780.

[18] G. Dushaq, A. Nayfeh, and M. Rasras, "Complementary metal oxide semiconductor (CMOS) compatible gallium arsenide metal-semiconductor-metal photodetectors (GaAs MSMPDs) on silicon using ultra-thin germanium buffer layer for visible photonic applications," *J Appl Phys*, vol. 126, no. 19, Nov. 2019, doi: 10.1063/1.5120705.

[19] R. Jones *et al.*, "Heterogeneously Integrated InP\/Silicon Photonics: Fabricating Fully Functional Transceivers," *IEEE Nanotechnol Mag*, vol. 13, no. 2, pp. 17–26, Apr. 2019, doi: 10.1109/MNANO.2019.2891369.

[20] I. A. Ukaegbu and H.-H. Park, "The design of Si-based Fresnel-zone lens for 3D IC optical interconnect applications," in *Smart Photonic and Optoelectronic Integrated Circuits XXII*, S. He and L. Vivien, Eds., SPIE, Feb. 2020, p. 72. doi: 10.1117/12.2541816.

[21] P. Steglich, S. Bondarenko, C. Mai, M. Paul, M. G. Weller, and A. Mai, "CMOS-Compatible Silicon Photonic Sensor for Refractive Index Sensing Using Local Back-Side Release," *IEEE Photonics Technology Letters*, vol. 32, no. 19, pp. 1241–1244, Oct. 2020, doi: 10.1109/LPT.2020.3019114.

[22] D. Dodane, J. Bourderionnet, S. Combrié, and A. de Rossi, "Fully embedded photonic crystal cavity with Q=06 million fabricated within a full-process CMOS multiproject wafer," *Opt Express*, vol. 26, no. 16, p. 20868, Aug. 2018, doi: 10.1364/OE.26.020868.

[23] F. Segovia-Chaves and H. Vinck-Posada, "Photonic band structure in square and triangular lattices of cylindrical-shell rods," *Optik (Stuttg)*, vol. 181, pp.

1013–1018, Mar. 2019, doi: 10.1016/j.ijleo.2018.12.127.

[24] F. Yang, Z. Ma, and X. Guo, "Bandgap characteristics of the two-dimensional missing rib lattice structure," *Appl Math Mech*, vol. 43, no. 11, pp. 1631–1640, Nov. 2022, doi: 10.1007/s10483-022-2923-6.

[25] A. Deyasi, U. Dey, S. Das, S. De, and A. Sarkar, "Computing Photonic Bandgap from Dispersion Relation for TM Mode Propagation Inside Metamaterial-Based 1D PhC," *Micro and Nanosystems*, vol. 12, no. 3, pp. 201–208, Dec. 2020, doi: 10.2174/1876402912666200130153324.

[26] Y. Tang, A. M. Mintairov, J. L. Merz, V. Tokranov, and S. Oktyabrsky, "Characterization of 2D-photonic crystal nanocavities by polarization-dependent photoluminescence," in *5th IEEE Conference on Nanotechnology, 2005.*, 2005, pp. 35–38 vol. 1. doi: 10.1109/NANO.2005.1500685.

[27] T. Iwaya, S. Ichikawa, M. Murakami, D. Timmerman, J. Tatebayashi, and Y. Fujiwara, "Design considerations of III-nitride-based two-dimensional photonic crystal cavities with crystallographically induced disorder," *Applied Physics Express*, vol. 14, no. 12, p. 122002, Dec. 2021, doi: 10.35848/1882-0786/ac3545.

[28] Z. Manzoor, V. Mkhitaryan, M. D. Sinanis, O. Yesilyurt, D. Peroulis, and A. V. Kildishev, "Employing Topological Properties of Phase Singularities for Designing Supercavity Systems with Tailored Excitation," *Advanced Physics Research*, Feb. 2023, doi: 10.1002/apxr.202200052.

[29] A. Mock and J. D. O'Brien, "Quality Factor Dependence on Vertical Slab Structure in Photonic Crystal Double Heterostructure Resonant Cavities," in *Advances in Optical Sciences Congress*, Optica Publishing Group, 2009, p. IMF2. doi: 10.1364/IPNRA.2009.IMF2.

[30] M. Minkov, V. Savona, and D. Gerace, "Photonic crystal slab cavity simultaneously optimized for ultra-high Q/V and vertical radiation coupling," *Appl Phys Lett*, vol. 111, no. 13, Sep. 2017, doi: 10.1063/1.4991416.

[31] I. Bahaddur, M. R. Tejaswini, S. Kumar T.C., P. Sharan, and P. C. Srikanth, "2D Photonic Crystal Cantilever Resonator Pressure Sensor," in *2019 Workshop on Recent Advances in Photonics (WRAP)*, 2019, pp. 1–4. doi: 10.1109/WRAP47485.2019.9013843.